Analysis of Single-RF MIMO Receiver with Beam-Switching Antenna

Donghyuk Gwak, Illsoo Sohn, and Seung Hwan Lee

This paper proposes a single-RF MIMO receiver that adopts a beam-switching antenna (BSA) instead of a conventional array antenna. The beauty of the proposed single-RF MIMO receiver with BSA is that it can be deployed in a very small physical space while achieving a full spatial multiplexing gain. Our analysis has revealed that the use of a BSA inevitably results in the spectrum spreading effect at the RF output, which in turn causes an SNR decrease and adjacent channel interference (ACI). Two novel receiver techniques are proposed to mitigate the issues of redundant sub-band suppression and ACI avoidance. Numerical analysis results verify the performance improvement from the proposed receiver techniques.

Keywords: MIMO, beam-switching antenna, single-RF MIMO receiver, parasitic antenna element, spread spectrum, compact MIMO.

I. Introduction

There have recently been significant efforts to reduce the physical size of multiple-input and multiple-output (MIMO) antennas. Some early works on MIMO antennas [1]–[2] have considered the use of a switched antenna array (SAA) as opposed to the conventional uniform linear array (ULA). SAAs implement a single RF front-end with multiple switchable antenna elements. Thus, SAAs have helped impact upon the size, weight, power consumption, and cost of the RF systems they employ. However, the extent to which the physical size of an RF system that employs an SAA can be reduced is limited because a minimum spacing is still required of antenna elements (for example, half a wavelength) to retain the benefits of MIMO. This is a critical obstacle to the deployment of MIMO in user devices.

In an effort to further reduce the physical size of MIMO transceivers, there has been an attempt to use only a single antenna element as well as a single RF front-end [3]–[5]. This class of antennas enables MIMO by changing beam patterns with multiple parasitic elements, and as such, these antennas are known as beam-steerable antennas. A typical implementation of a beam-steerable antenna is deploying a single active antenna element and several parasitic elements placed circularly surrounding the active antenna element. Figure 1 depicts a typical example of such a beam-steerable antenna (one with a single antenna element and six parasitic elements). The main advantage of this antenna structure is that it can exploit those properties of MIMO that are deemed desirable even in a very small physical space, which is a considerable improvement over ULAs and SAAs [6].

A beam-steerable antenna can be classified into two classes. One class is a beam-switching antenna (BSA), and the other

Manuscript received May 26, 2014; revised Mar. 3, 2015; accepted May 4, 2015.

This work was supported by Institute for Information & Communications Technology Promotion (IITP) grant funded by the Korea government (MSIP) (No. R0101-15-244, Development of 5G Mobile Communication Technologies for Hyper-connected Smart Services).

Donghyuk Gwak (gwakdh@etri.re.kr) and Seung Hwan Lee (corresponding author, lsh@etri.re.kr) are with the Communications & Internet Research Laboratory, ETRI, Daejeon, Rep. of Korea.

Illsoo Sohn (illsoo.sohn@gachon.ac.kr) is with the Department of Electronic Engineering, Gachon University, Seongnam, Rep. of Korea.

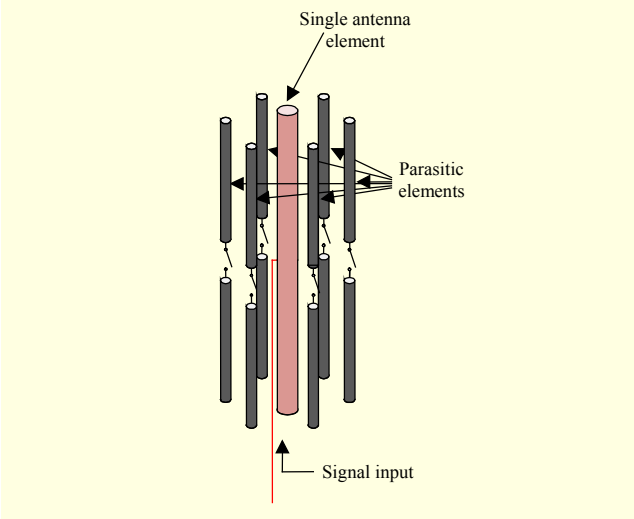

Fig. 1. Typical example of beam-steerable antenna.

is continuously varying beam pattern antenna. The main difference between the two classes is whether they change the beam patterns discretely or continuously. From an implementation point of view, the former is preferable owing to its simplicity.

For the application of a BSA at the transmitter side, a conceptual work was conducted in [7], followed by a single-RF transmitter implementation in [8]. It was demonstrated in the testbed that full spatial multiplexing gain can be achieved with a single-RF transmitter with a BSA, as with a conventional MIMO transmitter with a ULA [9]–[10].

For the application of a BSA at the receiver side, a method to achieve spatial multiplexing gain with an antenna that has a continuously varying beam pattern is introduced in [11]. In [11], a sampled rotating antenna is introduced to implement an effective single-RF MIMO receiver. However, it is very difficult to design and implement an antenna whose radiating pattern rotates in a continuous fashion. As an alternative, a single-RF MIMO receiver with BSA is proposed in [12] as a low-cost implementation form of a single-RF MIMO receiver.

We also consider the single-RF MIMO receiver with BSA, but focus on important practical issues that have not been extensively investigated in the literature. A BSA inevitably causes a spread of the received signal in the frequency spectrum. Since the spectrum spreading arises at the output of a BSA, a bandpass filter typically connected at the antenna element cannot control or mitigate the negative impacts from the spread spectrum. This means that a single-RF MIMO receiver with a BSA requires extra effort (see Section III-1) to deal with the spread spectrum.

The impact of the spread spectrum becomes very important since our main goal is to realize the implementation of our proposed single-RF MIMO receiver that adopts a BSA into user devices. In recent mobile cellular environments, available frequency resources below 3 GHz are very scarce so that adjacent bands are highly probable to be occupied and utilized. This implies that the signals in adjacent channels may induce out-of-band interference due to the spread spectrum. This type of interference scenario should be newly considered for the use of a BSA. Thus, we focus on the impact of out-of-band interferences that are inevitably induced by a BSA, which becomes a main hurdle.

In this paper, we propose a novel single-RF MIMO receiver with BSA that efficiently mitigates the aforementioned spread spectrum issues. This work includes an analysis of a single-RF MIMO receiver with BSA focusing particularly on spectrum spreading issues. The analysis reveals two major drawbacks of a single-RF receiver with BSA. One is the increase of noise power owing to the increased bandwidth of signals, decreasing the effective SNR. The other is the possible overlaps of the desired signal with adjacent signals during spreading. Based on the analysis, we propose two receiver techniques (that is, redundant sub-band suppression and adjacent channel interference (ACI) avoidance schemes) to mitigate the negative impacts from the spectrum spreading issues. The main goal of this paper is to investigate and resolve practical issues for deploying a BSA. Our simulation results verify that the proposed techniques effectively reduce the performance gap between the BSA and conventional ULA form of MIMO antennas. This is very appealing in the sense that a BSA requires only a single RF front-end and antenna element.

The remainder of this paper is organized as follows. In Section II, a beamspace domain representation of a MIMO channel and BSA receiver model are established. In Section III, an analysis on the characteristics of a BSA is conducted. In Section IV, two novel techniques for a BSA are introduced to improve the performance. Section V presents the simulation results. Finally, Section VI provides some concluding remarks regarding our proposal.

A summarizing list for frequently used variables is provided below to enhance readability:

- t: Time
- f: Frequency
- N_T: Total number of transmitting antennas
- M_R: Total number of receiving beam patterns
- φ_t: Angle of departure (AoD)
- φ_r: Angle of arrival (AoA)
- T_{sym}: Symbol duration
- f_{sym}: Symbol frequency
- f_c: Carrier frequency
- m: Index for receiving beams, $m = 1, 2, \ldots, M_R$
- l: Index for sub-bands of received signal $l = \ldots, -1, 0, 1, \ldots$
- l_{max}: The largest index of sub-band utilized

- l_{min}: The smallest index of sub-band utilized
- ρ: Signal-to-noise ratio (SNR)
- K: Switch-boosting factor
- L: Total number of sub-bands of interest $L = l_{max} - l_{min} + 1$

II. System Model

1. Beamspace Domain Representation

In the beamspace domain, the MIMO channel can be described by the channel gain matrix between the transmitting beam patterns and receiving beam patterns [13]. If the channel is time-invariant for the duration of interest, then the following equation, which represents a MIMO system, can be derived:

$$\mathbf{y}(t) = \mathbf{H}_{\text{bs}}\mathbf{x}(t) + \mathbf{v}(t), \tag{1}$$

where $\mathbf{x}(t)$ is an $N_T \times 1$ vector of the transmitting signals whose entries are normalized as $\mathrm{E}[\mathbf{x}\mathbf{x}^{\mathrm{H}}] = (P/N_T) \times \mathbf{I}_{N_T}$, P is total radiation power of a transmitting antenna, $\mathbf{v}(t)$ is an $M_R \times 1$ vector of ambient noise, $\mathbf{H}_{\text{bs}}$ is an $M_R \times N_T$ dimensional complex channel gain matrix, $\mathbf{y}(t)$ is an $M_R \times 1$ vector of the received signals, and $y_m(t)$ is the received signal when received through the mth receiving beam pattern.

Let us define $H_a(\varphi_t, \varphi_r)$ as the path attenuation; φ_t as the AoD; φ_r as the AoA; and $B_{t,n}(\varphi_t)$ and $B_{r,m}(\varphi_r)$ as the azimuthal complex directivity gain of the nth transmitting beam pattern and mth receiving beam pattern, respectively. The channel gain between the nth transmitting beam pattern and the mth receiving beam pattern, $\mathbf{H}_{\text{bs}}(m, n)$, can then be described as

$$\mathbf{H}_{\text{bs}}(m,n) = \frac{1}{4\pi^2}\oiint B_{r,m}{}^{*}(\varphi_r) H_a(\varphi_t, \varphi_r) B_{t,n}(\varphi_t)\,\mathrm{d}\varphi_t \mathrm{d}\varphi_r. \tag{2}$$

For simplicity, the beam patterns of a BSA are assumed to be mutually orthogonal. In addition, the path attenuation $H_a(\varphi_t, \varphi_r)$ is assumed to have zero autocorrelation except for identical AoA and AoD. Thus, the elements of the channel gain matrix $\mathbf{H}_{\text{bs}}$ are mutually independent circular symmetric complex variables.

This beamspace domain representation can also be applied to conventional MIMO antennas by specifying the transmitting or receiving beam pattern set. For example, a typical ULA MIMO transmitter whose inter-element distance is one-half of the wavelength can be modeled with beam patterns such that

$$B_{t,n}(\varphi_t) = e^{-\mathrm{j}2\pi\left(\frac{1}{2}(n-1)\sin\varphi_t\right)}. \tag{3}$$

Figure 2 shows the beamspace domain for a MIMO system with a conventional ULA transmitter and a BSA receiver.

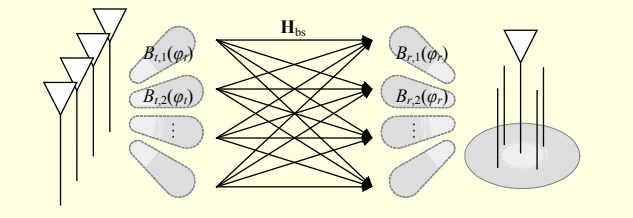

Fig. 2. Beamspace domain representation of MIMO system with ULA transmitter and BSA receiver.

2. BSA Receiver

A BSA receives a signal through a time-divisionally switching beam pattern. To exploit the spatial multiplexing gain, the BSA should switch its beam pattern into M_R patterns at least once for each pattern in a single symbol time, T_{sym}, which gives independent received signals $y_1(t)$, $y_2(t), \ldots, y_{M_R}(t)$. Here, we take the simplest case where the BSA equivalently allocates time to each pattern once in a symbol time in a round-robin manner. The received signal of the BSA is

$$r(t) = \sum_{m=1}^{M_R}\sum_{i=-\infty}^{\infty} \Pi\left(\frac{t-(m-1)\frac{T_{\text{sym}}}{M_R} - iT_{\text{sym}}}{\frac{T_{\text{sym}}}{M_R}}\right) y_m(t), \tag{4}$$

where $\Pi(t)$ can be defined as

$$\Pi(t) = \begin{cases} 1 & \text{for } -\frac{1}{2} < t \le \frac{1}{2}, \\ 0 & \text{otherwise.} \end{cases}$$

Consequently, the received signal of a BSA is equivalent to the time-multiplexed output of the elements of $\mathbf{y}(t)$.

III. Performance Analysis of Single-RF MIMO Receiver with BSA

1. Spread Spectrum Characteristics

To achieve spatial multiplexing gain with a BSA receiver, the beam-switching frequency of the BSA should be much higher than both the symbol rate and the bandwidth, which inevitably results in a spectrum spread in the frequency domain. The spectrum spread is undesirable in general, but here, we propose novel receiver processing schemes that extract a required transmitted signal from the spread spectrum efficiently.

The frequency-domain representation of the received signal can be obtained by a Fourier transform of the received signal as follows:

$$R(f)=\sum_{m=1}^{M_{\mathrm{R}}}\left[\left\{e^{-\mathrm{j}2\pi\frac{m-1}{M_{\mathrm{R}}}\frac{f}{f_{\mathrm{sym}}}}\frac{1}{M_{\mathrm{R}}}\mathrm{sinc}\left(\frac{f}{M_{\mathrm{R}}f_{\mathrm{sym}}}\right)\sum_{l=-\infty}^{\infty}\delta\left(f-lf_{\mathrm{sym}}\right)\right\}*Y_m(f)\right], \tag{5}$$

where f_{sym} is a symbol rate equal to $1/T_{\mathrm{sym}}$ [14]. The derivation details are presented in the Appendix. Further simplification of the frequency-domain representation is

$$R(f)=\sum_{m=1}^{M_{\mathrm{R}}}\left[\left\{\sum_{l=-\infty}^{\infty}e^{-\mathrm{j}2\pi\frac{m-1}{M_{\mathrm{R}}}l}\frac{1}{M_{\mathrm{R}}}\mathrm{sinc}\left(\frac{l}{M_{\mathrm{R}}}\right)\delta\left(f-lf_{\mathrm{sym}}\right)\right\}*Y_m(f)\right]. \tag{6}$$

Note that $Y_m(f)$ is a linear combination of transmitted signals, and its carrier frequency and bandwidth are identical to those of the transmitted signals represented by $\mathbf{x}(t)$. Thus, $R(f)$ can be decomposed into non-overlapping sub-band components.

We can sketch the power spectral density (PSD) of the BSA output from the result of (6). It has a sinc-squared function as an estimation line of the envelope. The main lobe of the sinc-squared function has $2M_{\mathrm{R}}-1$ sub-bands in it, and other side lobes have $M_{\mathrm{R}}-1$ sub-bands in them.

Let us define $W_l(f)$ as the frequency-shifted output of the sub-band component whose center frequency is $f_{\mathrm{c}}+lf_{\mathrm{sym}}$.

$$W_l(f)=\begin{cases}R\left(f-lf_{\mathrm{sym}}\right) & \text{for } \| f-f_{\mathrm{c}} \| \le \dfrac{f_{\mathrm{sym}}}{2},\\ 0 & \text{otherwise.}\end{cases} \tag{7}$$

From (6), we can find the fact that each $W_l(f)$ can be represented by a linear combination of $Y_m(f)$, and the equation also indicates that $W_l(f)$ is a linearly scaled value of $W_{\mathrm{mod}(l,M_{\mathrm{R}})}(f)$. This implies that the maximum number of independent sub-band components cannot go beyond M_{R}. The best strategy is to extract M_{R} sub-bands that are nearest to the center frequency to maximize the SNR, because other sub-band components are replicas of the centermost M_{R} sub-bands but with a lower PSD.

2. Capacity Analysis

The previous subsection described how the signal at the BSA output is spread. Here, we prove the feasibility of the transmitted signals being successfully reconstructed from the selected sub-band components of the BSA output. A capacity analysis follows.

Let $\mathbf{W}(f)$ be an $M_{\mathrm{R}}\times 1$ vector composed of the M_{R} centermost sub-band components.

$$\mathbf{W}(f)=\left[W_{l_{\min}}(f),\ldots,W_{l_{\max}}(f)\right]^{\mathrm{T}}, \tag{8}$$

where

$$\left(l_{\min},l_{\max}\right)=\begin{cases}\left(-\dfrac{M_{\mathrm{R}}-1}{2},\dfrac{M_{\mathrm{R}}-1}{2}\right) & M_{\mathrm{R}}\text{ is odd,}\\ \left(-\dfrac{M_{\mathrm{R}}}{2}+1,\dfrac{M_{\mathrm{R}}}{2}\right) & M_{\mathrm{R}}\text{ is even.}\end{cases}$$

Additionally, let $\mathbf{G}$ be a transfer function matrix between $\mathbf{Y}(f)$ and $\mathbf{W}(f)$; $\mathbf{W}(f)$ can then be represented as

$$\mathbf{W}(f)=\mathbf{G}\mathbf{Y}(f)=\mathbf{G}\mathbf{H}_{\mathrm{bs}}\mathbf{X}(f)+\mathbf{V}'(f), \tag{9}$$

where

$$\mathbf{G}=\frac{1}{M_{\mathrm{R}}}\mathbf{\Lambda}\mathbf{\Gamma},$$

$$\mathbf{\Lambda}=\mathrm{diag}\left(\mathrm{sinc}\left(\frac{l_{\min}}{M_{\mathrm{R}}}\right),\ldots,\mathrm{sinc}\left(\frac{l_{\max}}{M_{\mathrm{R}}}\right)\right),$$

$$\mathbf{\Gamma}=\begin{bmatrix}1 & \gamma^{l_{\min}} & \cdots & \gamma^{(M_{\mathrm{R}}-1)l_{\min}}\\ \vdots & \vdots & \ddots & \vdots\\ 1 & 1 & \cdots & 1\\ \vdots & \vdots & \ddots & \vdots\\ 1 & \gamma^{l_{\max}} & \cdots & \gamma^{(M_{\mathrm{R}}-1)l_{\max}}\end{bmatrix},$$

$$\gamma=e^{-\mathrm{j}2\pi\frac{1}{M_{\mathrm{R}}}}.$$

The elements of $\mathbf{V}'(f)$ in (9) are the time-multiplexed outputs of the thermal noise vector $\mathbf{v}(t)$; thus, each element has the same spectral characteristics as those of the thermal noise, $V(t)$.

Note that $\mathbf{\Gamma}$ is a scalar multiple of the unitary matrix, $\mathbf{\Lambda}$ is a diagonal matrix, and matrix $\mathbf{G}\mathbf{H}_{\mathrm{bs}}$ is non-singular as long as the spatial channel profile is not ill-conditioned. By multiplying the inversion of $\mathbf{G}\mathbf{H}_{\mathrm{bs}}$ at both sides of (9), the transmitted signal can be reconstructed, achieving full spatial multiplexing gain.

The channel capacity of this system can be calculated as

$$C=\mathrm{E}\left[\log_2\det\left(\mathbf{I}_{M_{\mathrm{R}}}+\frac{P\mathbf{G}\mathbf{H}_{\mathrm{bs}}\mathbf{H}_{\mathrm{bs}}^{\mathrm{H}}\mathbf{G}^{\mathrm{H}}}{N_{\mathrm{T}}N_0W}\right)\right]. \tag{10}$$

With the well-conditioned channel matrix $\mathbf{H}_{\mathrm{bs}}$, which satisfies $\mathbf{H}_{\mathrm{bs}}\mathbf{H}_{\mathrm{bs}}^{\mathrm{H}}\cong N_{\mathrm{T}}\mathbf{I}_{M_{\mathrm{R}}}$,

$$C\cong\mathrm{E}\left[\log_2\det\left(\mathbf{I}_{M_{\mathrm{R}}}+\frac{\rho}{M_{\mathrm{R}}}\mathbf{\Lambda}^2\right)\right], \tag{11}$$

where

$$\rho=\frac{P}{N_0W}.$$

In (11), the term $1/M_{\mathrm{R}}$ implies a reduction of the received power that is comparable to that of a conventional MIMO receiver. This originates from the characteristics of a time-divisional receiver with a single active antenna. In addition, the term $\mathbf{\Lambda}^2$ implies a performance degradation coming from the switching of the beam pattern. A novel technique to mitigate this performance degradation is proposed in Section IV.

IV. Proposed BSA Receiver

1. SNR Improvement by Redundant Sub-band Suppression

The previous section discussed the performance degradation issues coming from the hard switching of the receiving beam patterns. To reduce this performance degradation, we propose a novel scheme called redundant sub-band suppression. Two different tasks should be accomplished. One is to minimize the powers of redundant replica sub-bands, and the other is to balance the power among the sub-bands of interest.

Given the number of receiving patterns, the power ratios between the replicas are deterministic. To assign a larger portion of power to the strongest replica, there is no choice but to increase M_{R}. However, the increment of M_{R} also implies an increased number of sub-bands. The proposed scheme suppresses the power of the sub-bands other than L sub-bands, which are mutually independent, $L \le M_{\mathrm{R}}$, by designating the shape of the receiving beam patterns into specific shapes.

Here, we provide an example of nullifying every sub-band except for the centermost L sub-bands and their duplicates. The number of sub-bands L is a configurable variable determining how many independent signals will survive after sub-band suppression. From (9), the following equation should be met to nullify the lth sub-band component:

$$\begin{bmatrix} 1 & \gamma^{l} & \cdots & \gamma^{(M_{\mathrm{R}}-1)l} \end{bmatrix} \mathbf{H}_{\mathrm{bs}} = \mathbf{0}_{1\times N_{\mathrm{T}}}. \tag{12}$$

Equation (12) holds true if the set of receiving beam patterns satisfies

$$\begin{bmatrix} 1 & \gamma^{l} & \cdots & \gamma^{(M_{\mathrm{R}}-1)l} \end{bmatrix} \begin{bmatrix} B_{r,1}(\varphi_r) \\ B_{r,2}(\varphi_r) \\ \vdots \\ B_{r,M_{\mathrm{R}}-1}(\varphi_r) \end{bmatrix} = 0. \tag{13}$$

In (13), there are M_{R} degrees of freedom in designing the receiving beam pattern set. Thus, it is affordable to design such a pattern set that nullifies multiple sub-bands at the same time.

Let us take as an example a case in which $M_{\mathrm{R}} = 20$ and $L = 4$. The simplest solution satisfying the condition of (13) is then

$$B_{r,m}(\varphi_r) = \sum_{l=-1}^{2} e^{-\mathrm{j}l(\varphi_r - 2\pi(m/M_{\mathrm{R}}))}. \tag{14}$$

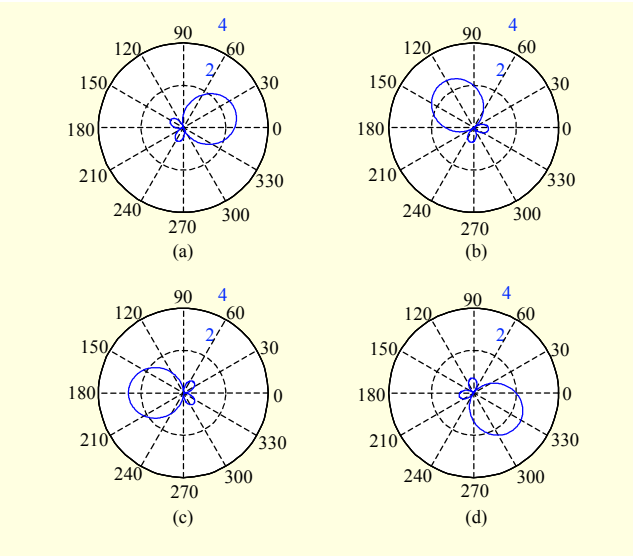

Fig. 3. Example of receiving beam patterns designated for sub-band suppression: (a) first beam pattern, (b) seventh beam pattern, (c) tenth beam pattern, and (d) eighteenth beam pattern.

Additionally, their graphical representation is depicted in Fig. 3. This beam pattern set is designated to allocate powers only on $W_{-1}(f)$, $W_0(f)$, $W_1(f)$, and $W_2(f)$.

The capacity of a system in which sub-band suppression is applied can be calculated as follows. Let us assume that the sub-bands of interest have the same power such that

$$\mathbf{\Gamma}\mathbf{H}_{\mathrm{bs}}\mathbf{H}_{\mathrm{bs}}{}^{\mathrm{H}}\mathbf{\Gamma}^{\mathrm{H}} \cong N_{\mathrm{T}}{}^{2}\frac{M_{\mathrm{R}}}{L}\begin{bmatrix} \mathbf{0} & \cdots & \mathbf{0} \\ \vdots & \mathbf{I}_{L} & \vdots \\ \mathbf{0} & \cdots & \mathbf{0} \end{bmatrix}. \tag{15}$$

The assumption implied in (15) is that the entries of $\mathbf{W}$, except for the L centermost sub-bands, are cancelled out and the received power is equally redistributed on the L centermost sub-bands. This assumption holds true if the receiving beam patterns are designed in a way that satisfies (13). With the assumption, the capacity of a system in which sub-band suppression is computed by combining (9) and (10) with (15) is as follows:

$$C = \mathrm{E}\left[\log_2 \det\left(\mathbf{I}_{M_{\mathrm{R}}} + \frac{N_{\mathrm{T}}\rho}{M_{\mathrm{R}}L}\mathbf{\Lambda}'^{2}\right)\right], \tag{16}$$

where

$$\mathbf{\Lambda}' = \mathrm{diag}\left(\mathbf{0}_{l'_{\min}-l_{\min}}, \mathrm{sinc}\left(\frac{l'_{\min}}{M_{\mathrm{R}}}\right), \cdots, \mathrm{sinc}\left(\frac{l'_{\max}}{M_{\mathrm{R}}}\right), \mathbf{0}_{l_{\max}-l'_{\max}}\right).$$

The meaning of (16) is that by manipulating receiving beam

patterns, a BSA can suppress power allocation on unwanted sub-bands. And a BSA allocates saved power on sub-bands of interest instead. The diagonal submatrix in $\mathbf{\Lambda}'$ converges into $\mathbf{I}_L$ in the case of $M_R \gg L$. This implies that the negative effect of hard switching nearly vanishes. It seems to be clearly helpful to increase the number of receiving beam patterns; however, increasing the number of receiving beam patterns requires increasing the number of parasitic elements with higher hardware costs.

In short, the proposed scheme underutilizes the maximum number of independent paths intentionally to remove the negative effect coming from the beam switching. In an ideal case where hardware costs are not of a major concern, the proposed sub-band suppression scheme can achieve a channel capacity close to the theoretical capacity upper bound for given SNR by deploying a large number of parasitic elements.

2. ACI Avoidance

A BSA spreads its received signal in the frequency spectrum. If any undesired signals exist on an adjacent channel, then a BSA receiver will spread the spectra of both signals simultaneously, which may result in a spectrum overlapping of the desired and undesired signals. In addition, it may severely harm the SINR of the received signal. We propose a novel ACI avoidance scheme for mitigating this effect. We attempt to relocate the spectrum of a BSA received signal by multiplying the switching frequency by factors of K, $K \in \mathbb{N}$. The received signal of a BSA is

$$r^{(K)}(t) = \sum_{m=1}^{M_R} \sum_{i=-\infty}^{\infty} \Pi\left(\frac{t-(m-1)\frac{T_{sym}}{KM_R} - i\frac{T_{sym}}{K}}{\frac{T_{sym}}{KM_R}} \right) y_m(t). \quad (17)$$

Additionally, its frequency domain can be represented as

$$R^{(K)}(f) = \sum_{m=1}^{M_R} \left[\left\{ \sum_{l=-\infty}^{\infty} e^{-j2\pi\frac{m-1}{M_R}l} \frac{1}{M_R} \mathrm{sinc}\left(\frac{1}{M_R}\right) \delta\left(f - lKf_{sym}\right) \right\} * Y_m(f) \right]. \quad (18)$$

The results of the proposed ACI avoidance scheme, which is represented by (18), include the sub-band components, which are identical to those of the original BSA spectrum except for their center frequency and broadened frequency spacing among them. Figure 4 shows a flowchart exemplifying the ACI avoidance algorithm, which was devised to take advantage of the previously described spectrum relocation phenomenon.

If a receiver has prior knowledge of the PSD of both the desired signal and the adjacent channel signal, then the receiver can predict how both spectra will spread. It is then possible to calculate the SINR expectation of each sub-band when switch-boosting factor K is chosen. The algorithm searches for M_R mutually independent sub-bands with the highest SINR from all possible sub-bands.

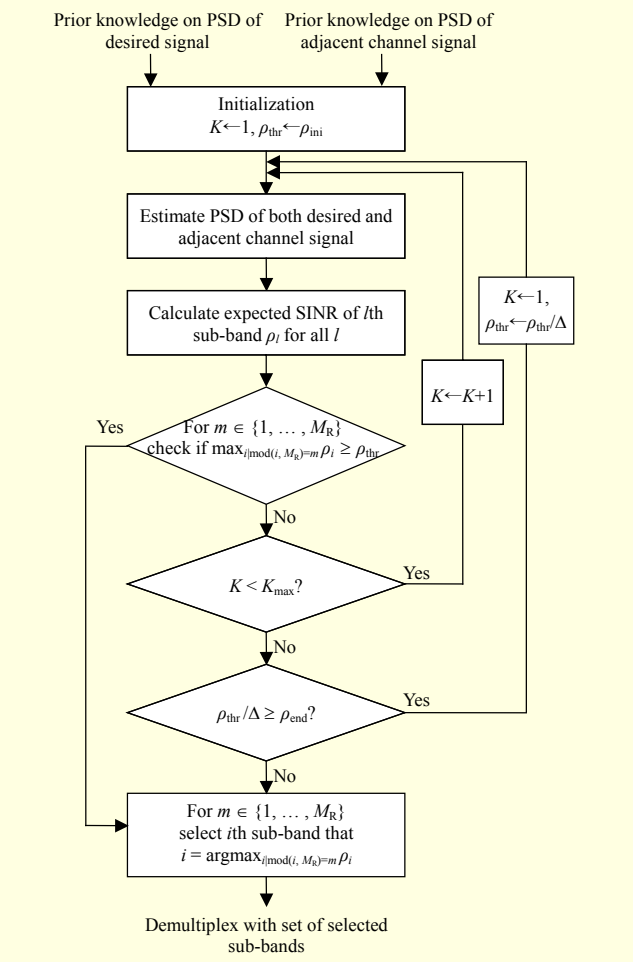

Fig. 4. Flowchart exemplifying ACI avoidance algorithm.

Since $W_l(f)$ is a linearly scaled replica of $W_{\mathrm{mod}(l,M_R)}(f)$, the set of sub-bands

$$S_a := \{W_l(f) \mid \mathrm{mod}(l, M_R) = a\} \quad (19)$$

contains replicas of $W_a(f)$. Moreover, there are only M_R of such sets $S_0, \dots, S_{M_R-1}$ because S_a is an identical set with set $S_{\mathrm{mod}(a,M_R)}$. Thus, it is natural to collect M_R sub-bands by picking the sub-band with the highest SINR from each set S_a.

When the chosen sub-band cannot meet the minimum SINR threshold, ρ_{thr}, the algorithm increases K by one and the process is repeated. If an appropriate subset is not found while sweeping the value of K from one to K_{max}, then the value of ρ_{thr} is reduced by a factor of Δ and the process is repeated. The value of ρ_{thr} starts from ρ_{ini} and ends before being less than ρ_{end}.

The overall complexity of this algorithm is $O\left(K_{\max}\left\lfloor \log_{\Delta}\frac{\rho_{\text{ini}}}{\rho_{\text{end}}}\right\rfloor \chi\right)$, where χ is the number of sub-bands in a window for SNR comparison.

By deploying the proposed algorithm, a BSA can prevent undesirable spectral overlapping. The algorithm enables the system to mitigate interference coming from an adjacent channel as long as there are appropriate idle bands needed for spectrum relocation. The proposed algorithm requires high-frequency switching devices and a high-speed analog-to-digital converter. This may induce additional hardware costs. However, achievements in contemporary device technology have made this inexpensive.

V. Simulation Results

1. Spectral Analysis

A spectral analysis is conducted upon simulation to confirm the nature of the spectrum spreading of the BSA received signal. Multiple streams of 16 QAM are generated and transmitted by the transmitter. Table 1 describes the system parameter configurations used in the simulation.

Figure 5 shows the received signal spectrum of the BSA receiver averaged over 100 time-invariant channel realizations when $M_R = 4$. The solid line indicates the PSD of a BSA received signal, and the dotted line indicates the analytically derived envelope for PSD. We find that the PSD of the BSA is well-fitted to the envelope to reconfirm the results of analysis.

There are lobes in the envelope whose null-to-null bandwidths are identical to the beam-switching frequency $M_R f_{\text{sym}}$ (in particular, the main lobe is twice as wide). There are $M_R - 1$ sub-bands embedded in each lobe (in particular, there are $2M_R - 1$ sub-bands for the main lobe); each sub-band has a bandwidth of f_{sym}. It is hard to visually identify sub-bands from the PSD of Fig. 5, since there is no null band between sub-bands. However, we can still try to imagine $2M_R - 1$ sub-bands embedded within the main lobe in a fully packed manner.

The spatial multiplexing can be achieved from any of the M_R sub-bands, which are carrying mutually independent information. From the analysis done in Section III, we know that the mutual independence among the chosen sub-bands will only hold if the indices of the chosen sub-bands all have different values once they have been divided by M_R. If interference is not considered, then it is optimal to pick M_R sub-bands from the centermost sub-bands in the main lobe. Since a BSA utilizes M_R sub-bands from a received signal, the observation bandwidth is widened by M_R. Accordingly, the total noise increases by M_R, and SNR degrades by M_R compared to that of the conventional MIMO receiver. Moreover, as the received power is unequally distributed on those sub-bands, a slight additional effective SNR degradation is expected. Since this additional degradation can be resolved by redundant sub-band suppression, the quantitative analysis on it will be introduced in the following subsection to avoid duplication here.

Table 1. System parameter configurations for simulation.

Parameter	Set value
f_c	1 GHz
f_{sym}	10 MHz
N_r	4
M_R	4
Ergodic mean Rx power	–74 dBm
Noise density	–174 dBm/Hz
Modulation scheme	BPSK
Number of symbols sent	100

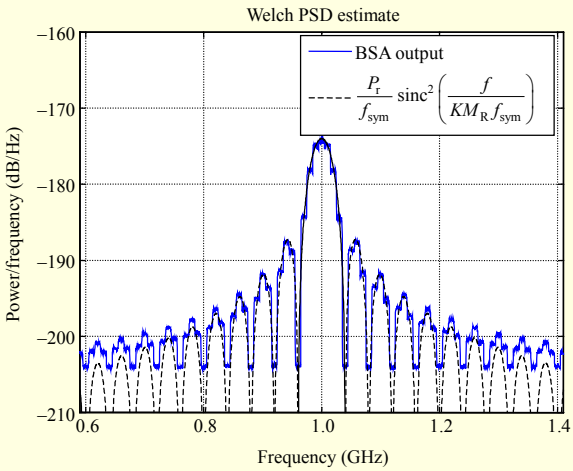

Fig. 5. PSD of BSA output with mutually orthogonal receiving beam pattern set.

2. Redundant Sub-band Suppression

The performance of the MIMO system featuring a ULA transmitter and BSA receiver is compared with that of a conventional MIMO system in Fig. 6. Both systems operate a 4 by 4 MIMO with full multiplexing mode. The solid line indicates the capacity of the conventional MIMO in a Rayleigh fading channel, and the dotted line represents the capacity of the MIMO system with a ULA-BSA pair. The dashed line represents the capacity of the MIMO system with a ULA-BSA pair when the proposed redundant sub-band suppression scheme is applied. For this system, M_R is set to

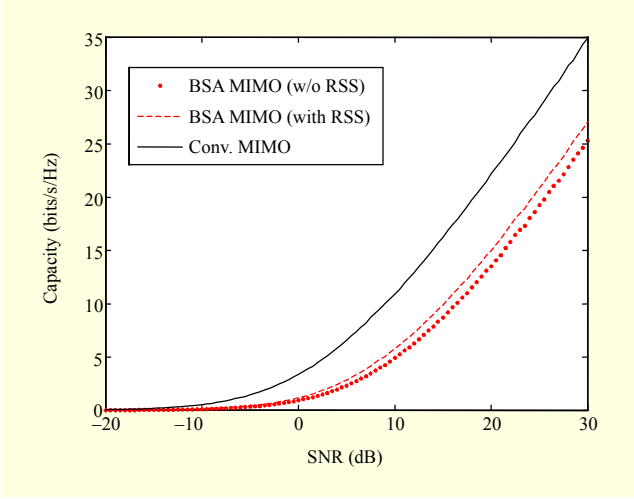

Fig. 6. MIMO capacity performance comparison.

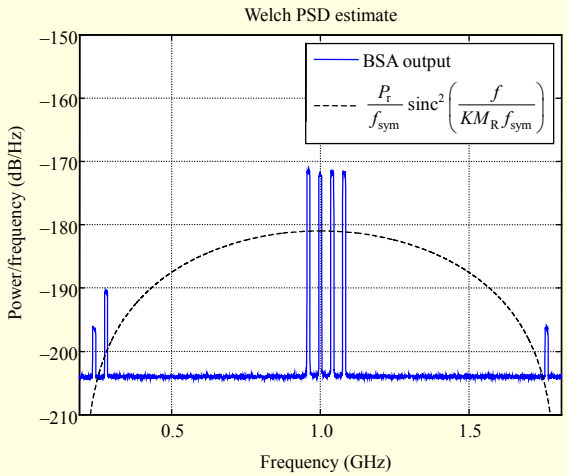

Fig. 7. PSD of signal received by BSA with sub-band suppression technique (when $L = 4$ and $K = 5$).

20 and L is set to 4.

From Fig. 6, we can conclude that a BSA with full multiplexing mode performs properly because the capacity curve of a BSA has the same slope as that of a conventional MIMO in high SNR regions. Since a BSA receiver uses signals from the L sub-bands, which means an L-times broader observation bandwidth, it receives L-times higher noise. Hence, there inevitably exists an L-fold SNR degradation too. However, the dashed line shows that the SNR degradation can be relieved with the deployment of the proposed redundant sub-band suppression scheme.

The amount of SNR degradation for the "BSA MIMO w/o RSS" and "BSA MIMO with RSS" cases can be derived by comparing Shannon's capacity with (11) and (16), respectively, which are $1/M_R^2 \sum_{l=l_{min}}^{l_{max}} \text{sinc}^2(l/M_R)$ for the "BSA MIMO w/o RSS" case and $1/M_R L \sum_{l=l'_{min}}^{l'_{max}} \text{sinc}^2(l/M_R)$ for the "BSA MIMO with RSS" case. Assuming $M_R \gg 1$ and $M_R \gg L$, $1/M_R^2 \sum_{l=l_{min}}^{l_{max}} \text{sinc}^2(l/M_R)$ approaches to $1/M_R \times \int_{-\frac{1}{2}}^{\frac{1}{2}} \text{sinc}^2(\pi x)\, dx \cong 0.7737/M_R$, and $1/M_R L \sum_{l=l'_{min}}^{l'_{max}} \text{sinc}^2(l/M_R)$ approaches to $1/L$. This analysis fits well with our simulation results depicted in Fig. 6. The conformity between the simulation results and analysis is proven by the fact that the SNR-capacity curves of BSA "without RSS" or "with RSS" are each right-shifted from that of a conventional MIMO by approximately 7.135 dB and 6 dB, respectively.

Figure 7 shows the PSD of a BSA output when the proposed redundant sub-band suppression scheme is applied. This exemplifies the case in which M_R is set to 20 and L is set to 4. High-speed beam switching is applied here to make the sub-bands in Fig. 7 visually easily identifiable. It shows that all redundant sub-bands except for four centermost sub-bands are effectively cancelled out. In addition, the graph indicates that the power distribution is concentrated on the four centermost sub-bands, as expected.

The meaning of this result is as follows. First, the BSA with RSS scheme equalizes power distribution among the centermost sub-bands by increasing the number of beam patterns. Second, it suppresses the power of out-of-interest sub-bands by adopting a designated beam pattern set. As a result, the suppressed power will be distributed equally on those sub-bands that are of-interest. By means of sacrificing a full multiplexing gain that is identical to the number of beam patterns M_R, it achieves a multiplexing gain of L while mitigating effective SNR degradation coming from unequal power distribution among the chosen sub-bands.

3. ACI Avoidance with High-Speed Beam Switching

The simulation results of the proposed ACI avoidance scheme have been presented. For simplicity, we assume that only one adjacent channel signal exists. The center frequency of the adjacent signal is located in $2f_{sym}$, far from the center frequency of the desired signal. In addition, the adjacent channel signal occupies a bandwidth that is twice that of the desired signal. Figure 8(a) shows that the spectra of the signal and interference plus thermal noise can be received by an omni-directional antenna if it is replaced with a BSA.

Figure 8(b) shows the spectra of the signal and interference plus thermal noise when $K = 5$, which presents a case in which a BSA avoids adjacent interference successfully with a five-

ETRI Journal, Volume 37, Number 4, August 2015
http://dx.doi.org/10.4218/etrij.15.0114.0618

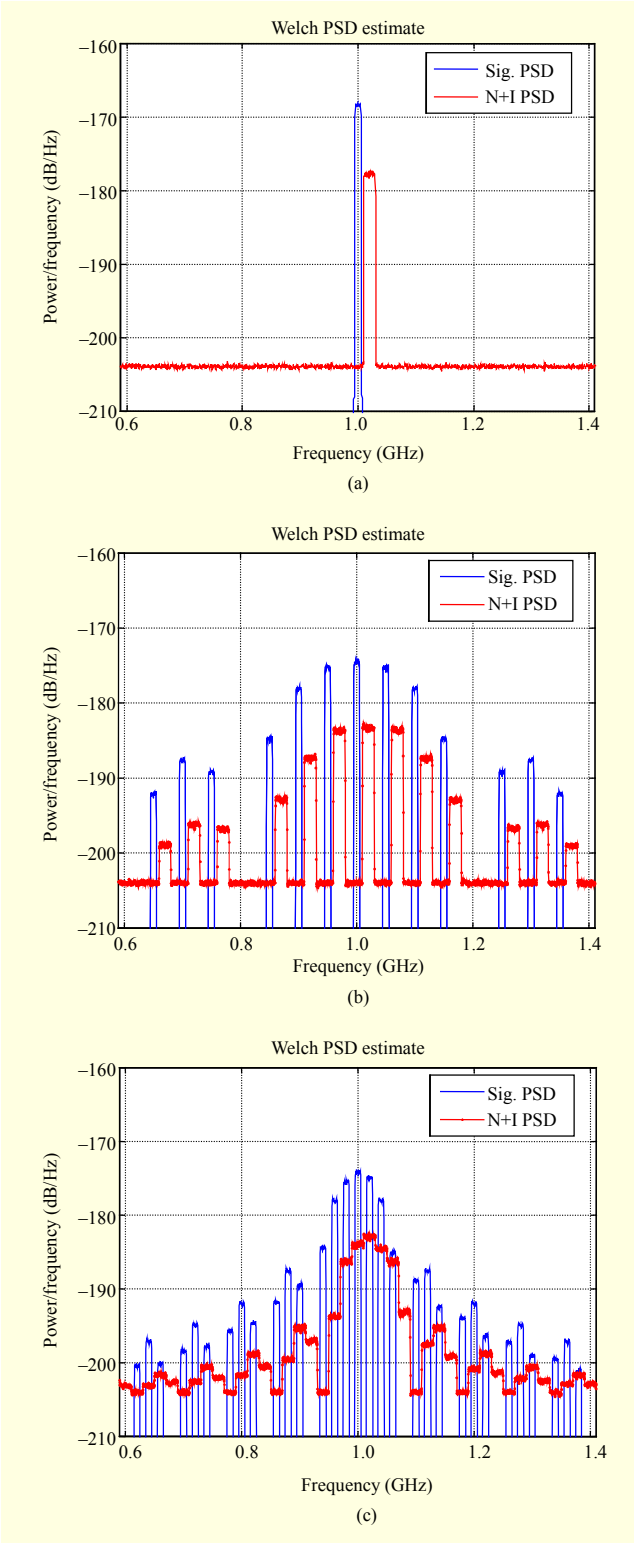

Fig. 8. Spectra of signal and interference plus thermal noise: measured by (a) omni-directional single antenna, (b) BSA when $K = 5$, and (c) BSA when $K = 2$.

fold broadened frequency spacing between sub-bands. Finally, Fig. 8(c) shows the spectra of the signal and interference plus thermal noise when $K = 2$, where the BSA fails to avoid adjacent interference because the frequency spacings between sub-bands are not sufficiently spread owing to the small value of K. Table 2 shows the BER performance comparison between the results of the two ACI avoidance cases.

Table 2. BER performance of BSA receiver in presence of ACI (BPSK, $E_b/N_0 = 30$ dB, and $M_R = 4$).

	$K = 5$	$K = 2$
BER	0.0002	0.1020

The fact that the high-speed beam switching technique is able to avoid any adjacent interference is significant because a BSA is fragile to interference signals existing in adjacent bands. This technique grants a BSA a means to mitigate ACI, while costing nothing but requiring the capability of high-frequency switching.

VI. Conclusion

In this paper, we showed that spatial multiplexing gain can be achieved using a single-RF MIMO receiver with BSA. Though a spatial multiplexing gain equivalent to that achievable with a conventional MIMO receiver is possible, it comes at the cost of additional SNR degradation. Despite this, a BSA can be still an attractive implementation form for a MIMO receiver, since it has a small physical size and can help reduce the number of RF front-ends. An in-depth study conducted on the frequency spreading characteristics of a single-RF MIMO receiver with BSA revealed the relations between transmitted signals and the sub-bands of a BSA output signal. It was also shown that the required condition for a full spatial multiplexing gain is the non-singularity of the beamspace MIMO channel matrix.

Two novel receiver techniques were proposed so that a BSA may enhance its performance. To eliminate the negative effect of ACI, a high-speed beam switching method is proposed. This scheme relocates the spectrum of a BSA by increasing the beam-switching frequency without increasing the number of beam patterns. This results in broadened frequency spacing between sub-bands such that the spectrum of the desired signal can mitigate ACI effectively. Furthermore, we proposed a redundant sub-band suppression scheme to reduce SINR degradation. This scheme enhances the SINR of a BSA by nullifying the redundant sub-bands that have a low SINR profile. With the precomputed receiving beam pattern set, the SNR is effectively improved.

References

[1] S. Henault, B.R. Jackson, and Y.M.M. Antar, "Compensation of Time-Division Multiplexing Distortion in Switched Antenna Arrays with a Single RF Front-End and Digitizer," *IEEE Trans. Antennas Propag.*, vol. 61, no. 8, Aug. 2013, pp. 4383–4388.

[2] J.D. Fredrick, Y. Wang, and R. Itoh, "A Smart Antenna Receiver Array Using a Single RF Channel and Digital Beamforming," *IEEE Trans. Microw. Theory Techn.*, vol. 50, no. 12, Dec. 2002, pp. 3052–3058.

[3] A. Sayeed and N. Behdad, "Continuous Aperture Phased MIMO: Basic Theory and Applications," *Conf. Commun., Contr., Comput.*, Allerton, IL, USA, Sept. 29–Oct. 1, 2010, pp. 1196–1203.

[4] M. Wennstrom and T. Svantesson, "An Antenna Solution for MIMO Channels: The Switched Parasitic Antenna," *IEEE Int. Symp. Pers., Indoor Mobile Radio Commun.*, San Diego, CA, USA, vol. 1, Sept. 2001, pp. 159–163.

[5] K. Gyoda and T. Ohira, "Design of Electronically Steerable Passive Array Radiator (ESPAR) Antennas," *IEEE Antennas Propag. Soc. Int. Symp.*, Salt Lake City, UT, USA, vol. 2, July 16–21, 2000, pp. 922–925.

[6] Z. Jin, J.-H. Lim, and T.-Y. Yun, "Small-Size and High-Isolation MIMO Antenna for WLAN," *ETRI J.*, vol. 34, no. 1, Feb. 2012, pp. 114–117.

[7] A. Kalis, A.G. Kanatas, and C.B. Papadias, "A Novel Approach to MIMO Transmission Using a Single RF Front End," *IEEE J. Sel. Areas Commun.*, vol. 26, no. 6, Aug. 2008, pp. 972–980.

[8] O.N. Alrabadi et al., "A Universal Encoding Scheme for MIMO Transmission Using a Single Active Element for PSK Modulation Schemes," *IEEE Trans. Wireless Commun.*, vol. 8, no. 10, Oct. 2009, pp. 5133–5142.

[9] O.N. Alrabadi, J. Perruisseau-Carrier, and A. Kalis, "MIMO Transmission Using a Single RF Source: Theory and Antenna Design," *IEEE Trans. Antennas Propag.*, vol. 60, no. 2, Feb. 2012, pp. 654–664.

[10] O.N. Alrabadi et al., "Spatial Multiplexing with a Single Radio: Proof-of-Concept Experiments in an Indoor Environment with a 2.6 GHz Prototype," *IEEE Commun. Lett.*, vol. 15, no. 2, Feb. 2011, pp. 178–180.

[11] R. Bains and R. Muller, "Using Parasitic Elements for Implementing the Rotating Antenna for MIMO Receivers," *IEEE Trans. Wireless Commun.*, vol. 7, no. 11, Nov. 2008, pp. 4522–4533.

[12] M. Yoshida, K. Sakaguchi, and K. Araki, "Single Front-End MIMO Architecture with Parasitic Antenna Elements," *IEICE Trans. Commun.*, vol. E95-B, no. 3, Mar. 2012, pp. 882–888.

[13] V.I. Barousis, A.G. Kanatas, and A. Kalis, "Beamspace-Domain Analysis of Single-RF Front-End MIMO Systems," *IEEE Trans. Veh. Technol.*, vol. 60, no. 3, Mar. 2011, pp. 1195–1199.

[14] J.G. Proakis and D.K. Manolakis, "*Digital Signal Processing: Principles, Algorithms, and Applications*," 4th ed., Upper Saddle River, NJ, USA: Prentice Hall, 2007, pp. 841–843.

Donghyuk Gwak received his BS and MS degrees in the field of electrical engineering from Seoul National University, Rep. of Korea, in 2010 and 2013, respectively. Since 2013, he has been a researcher with the Electronics and Telecommunications Research Institute, Daejeon, Rep. of Korea. His research interests include beamforming, interference management, compressive sensing, and massive MIMO.

Illsoo Sohn received his BS, MS, and PhD degrees in 2003, 2005, and 2009, respectively, from Seoul National University, Rep. of Korea, all in the field of electrical engineering. He worked as a postdoctoral researcher at the University of Texas at Austin, USA, from 2009 to 2010. He worked as a senior research engineer at LG Electronics, Seoul, Rep. of Korea, from 2010 to 2012. He worked as a network design engineer at KT, Seongnam, Rep. of Korea, from 2012 to 2013. Since 2013, he has been an assistant professor at the Department of Electronic Engineering, Gachon University, Seongnam, Rep. of Korea. His current research interests include statistical inference, message-passing algorithms, multi-user MIMO, multi-cell MIMO, time division duplex, distributed antennas systems, and cross-layer optimization.

Seung Hwan Lee received his BS and MS degrees in the field of electrical engineering from Korea University, Seoul, Rep. of Korea, in 1995 and 1997, respectively and his PhD degree in digital communication from the University of Edinburgh, UK, in 2007. He has been with the Electronics and Telecommunications Research Institute since 2001 and is now leading the 5G project strategy team. His research includes multiuser scheduling, MIMO, cross-layer optimization, cognitive radio systems, and 5G systems.